Pergamon

Int. J. Heat Mass Transfer. Vol. 41, No. 3, pp. 563–573, 1998

Printed in Great Britain
0017-9310/98 $19.00+0.00

PII: S0017-9310(97)00149-X

Heat transfer in curved and straight channels with transitional flow

C. R. HEDLUND and P. M. LIGRANI†

Convective Heat Transfer Laboratory, Department of Mechanical Engineering, University of Utah, Salt Lake City, Utah 84112, U.S.A.

(*Received* 9 *September* 1996 *and in final form* 2 *May* 1997)

Abstract—Heat transfer in a channel with a straight portion followed by a portion with mild curvature is studied at Dean numbers from 300 to 750. The channel aspect ratio is 40, radius ratio is 0.979, and the ratio of shear layer thickness to channel inner radius is 0.011. Important Nusselt number increases occur due to a variety of laminar-to-turbulent transitional phenomena which occur mostly in the upstream straight portion of the channel but then continue to cause important variations in the downstream curved portion. Nusselt numbers from concave and convex surfaces with these transitional phenomena show the effects of curvature, streamwise development, Dean number, buoyancy and flow tripping. © 1997 Elsevier Science Ltd.

INTRODUCTION

Flows in curved and straight channels provide opportunities to study physical aspects of transition from laminar conditions. Transitions in these two types of channels are fundamentally different. Curved channels develop coherent secondary flows in the form of counter-rotating Dean vortex pairs which form across the entire channel span [1–3]. Straight pipes and channels generally develop regions of longitudinally distinct local instability referred to as 'slugs' and 'puffs' [4, 5]. Transitional flow phenomena in channels can be particularly complex, especially if they involve centrifugally induced arrays of vortex pairs [1–3] in combination with such 'puffs' or 'slugs' of local turbulence [4, 5]. The centrifugally-induced instabilities in curved channels are also distinct from instabilities found in boundary layers on curved surfaces and in Taylor–Couette passages. Channel flows are parallel open flows, whereas curved boundary layers and Taylor–Couette passage flows are weakly non-parallel open flows and parallel closed flows, respectively. Transition in channels is also important for a range of practical applications. These include cooling passages in gas turbine blades, internal combustion engine cooling ducts, heat exchangers, and fuel grain porting within hybrid rocket motors.

Several other studies examine the effects of curvature on heat transfer in channels with laminar and transitional flows. Cheng and Akiyama [6] describe a numerical treatment of heat transfer in curved channels with fully developed, laminar forced convection, no buoyancy, and constant heat flux boundary conditions. Channels are employed with aspect ratios of 0.2, 0.5, 1, 2 and 5. For $Pr = 0.73$, ratios of (perimeter-averaged) curved channel Nusselt number to straight channel Nusselt number range from 1.05 to 2.3 at the ends of their ducts. Cheng and Akiyama also provide evidence of secondary flows in pressure and velocity predictions over plane surfaces. Mori *et al.* [7] present experimental data for heat transfer in a square channel with a 220° curved section at Dean numbers from 150 to 5000. Boundary and flow conditions similar to Cheng and Akiyama [6]. The authors also present numerical results for fully developed conditions. For $Pr = 0.71$, measured and predicted ratios of (perimeter-averaged) curved channel Nusselt number to straight channel Nusselt number range from 2.3 to 20.0. For the square channel, measured Nusselt numbers agree with analytic results with laminar and turbulent flows. As for Cheng and Akiyama [6], Mori *et al.* [7] evidence secondary flows in pressure and velocity data. In another numerical description of curved channel heat transfer, Yee *et al.* [8] model steady laminar flow with constant wall temperature boundary conditions. They predict perimeter-averaged Nusselt numbers at the end of the curved section from 12 to 14. For ducts with 90° bends and aspect ratios of 1/3, 1, and 3, these correspond to ratios of curved channel Nusselt number to straight channel Nusselt number of approximately 2.5 to 3.9 near the ends of their ducts.

Chilukuri and Humphrey [9] predict the influences of buoyant forces aligned with and opposite to the bulk flow direction. Perimeter averaged Nusselt numbers near the end of the curved section range from 14 to 16. This corresponds to ratios of curved section Nusselt number to straight section Nusselt number from 3.9 to 4.4 for a channel with a 90° bend, an aspect ratio of 1, $Pr = 1$, and $De = 367$. Secondary flows are evidenced in the curved section for both

† Author to whom correspondence should be addressed.

NOMENCLATURE

d	channel thickness
De	Dean number $(Ud/\nu)\sqrt{d/r_i}$
D_H	hydraulic diameter
g	gravitational acceleration
Gr	Grashof number, $gl^3\beta\Delta t/\nu^2$
h	heat transfer coefficient, equation (1)
k	thermal conductivity
l	half-span of the channel
Nu	spanwise-averaged Nusselt number, equation (2)
Pr	Prandtl number
Re	Reynolds number, UD_H/ν
Re_d	Reynolds number, Ud/ν
r_i	inner radius of channel convex surface
r_o	outer radius of channel concave surface
t	time-averaged local temperature
t_m	mixed-mean temperature
t_w	local wall temperature
u	streamwise mean velocity
u^+	u/u_τ
u'	fluctuating streamwise velocity
U	bulk mean velocity
u_τ	friction velocity
x	streamwise distance from location where heating begins
X	streamwise distance from channel inlet at nozzle exit
y^+	Yu_τ/ν
Y	distance normal from the concave channel surface.
Z	spanwise distance from channel spanwise centerline.

Greek symbols

β	volumetric coefficient of thermal expansion
δ	shear layer thickness
ν	kinematic viscosity
Δt	$(t_w - t_m)$.

Superscript

$\bar{}$	time-average.

buoyancy-assisted and buoyancy-opposed conditions. Komiyama [10] presents predicted Nusselt numbers from fully developed curved channel flow. The ratio of curved section Nusselt number to straight section Nusselt number is about 1.4 to 2.8. The author employs aspect ratios of 0.8 to 5, with $De = 11$–320, $Pr = 0.71$, and constant wall heat flux boundary conditions. Komiyama predicts a marked increase in Nusselt number as the Dean number increases at the higher range of Dean numbers examined. This corresponds to the case where more than one pair of Dean vortex pairs are present across the channel span. Of all the numeric investigations [6–10], only Chilukiri and Humphrey [9] address the effects of buoyancy on curved channel heat flow. Of all known numerical investigations of transitional flows in curved channels, only Yee *et al.* [8] predict the streamwise development of Nusselt numbers and secondary motions. Ligrani *et al.* [11] examine effects of curvature on measured heat transfer in channels with fully developed, laminar forced convection. Constant heat flux boundary conditions are applied to the surfaces of the channel, which has an aspect ratio of 40, a bend of 180°, $Pr = 0.71$, and Dean numbers up to 300. The authors indicate that spanwise-averaged Nusselt numbers are always higher on the concave surface than on the convex at all streamwise locations in the curved section, except just after curvature begins. Differences just downstream of the beginning of curvature result from initial development of Dean vortex pairs near the concave surface [1–3], and the secondary flows and unsteadiness associated with them [3, 12]. Significant Nusselt number increases on the concave and convex surfaces also occur with x/d for $x/d > 158$ and $De > 150$ due to the twisting secondary instability [3, 13]. Ratios of curved to straight channel Nusselt numbers for fully developed flow range from 1.0 to about 1.7 [11].

In the present work, effects of different transitional events on the measured local Nusselt numbers are of interest at Dean numbers from 300 to 750. This range of Dean numbers corresponds to Re_d from 2057 to 5142, respectively, and to Re from 4114 to 10 284, respectively. The present study thus covers a different range of experimental conditions than addressed by Ligrani *et al.* [11]. In that study, fully developed laminar flow is always present at the inlet of the curved portion of the channel, and transitional events, such as Dean vortex pairs, are contained entirely in the curved portion of the channel. The present study uses the same channel employed by Ligrani *et al.* [11], and continues work described in that study by addressing the influences of a variety of transitional disturbances initially present upstream of the curved segment of the channel.

Included in the present study are descriptions of the influences of streamwise development, varying Dean number, curvature, buoyancy, and flow tripping on local Nusselt number behavior. Of the archival literature known to the authors, only Mori *et al.* [8] and Ligrani *et al.* [11] present *measured* heat transfer data from curved channels with laminar and/or transitional flows. The present work is thus important as it provides new information regarding effects of complex

transitional flows on channel heat transfer. Particular attention is devoted to the effects of different initial conditions at the entrance to the curved portion of the channel. These initial conditions are provided at this location by varying transitional phenomena which develop at different streamwise locations in the straight portion of the channel located just upstream. As such, the present results provide an important tool for the development of numeric codes for the prediction of complex elliptic flows.

EXPERIMENTAL APPARATUS AND PROCEDURES

Curved and straight channels

Detailed descriptions of the rectangular cross-section channel employed for the present study are given by Ligrani *et al.* [11] and Hedlund [14]. Dimensional details are also illustrated in Fig. 1. The channel is instrumented for heat transfer measurements, has a thickness d of 1.27 cm, an aspect ratio of 40, and is dimensionally similar to another transparent curved channel used for flow visualization and quantitative measurements of flow properties by Ligrani and Niver [3], and Ligrani *et al.* [12, 13]. The ratio of shear layer thickness to convex radius of curvature δ/r_i is 0.011 in the curved section, which indicates mild curvature.

Just downstream of the channel inlet, the flow is conditioned to reduce spatial non-uniformities using arrays of screens, honeycombs, and nozzle with a 20 to 1 contraction ratio. Figure 1 shows that the straight section is composed of an initial unheated section 0.57 m long followed by a heated section 1.52 m long. The straight section allows hydrodynamically and thermally fully developed channel flow to develop before entering the curved section under most conditions studied [11, 15]. The fluid then enters a 180° curved channel section with convex and concave surface radii of 59.69 and 60.96 cm. The interior walls of the heated section are made of 0.08 cm thick Lexan. Upon exiting the curved section, the flow enters a second straight section with a length of 2.44 m. As flow leaves the second straight portion, it passes through additional flow management devices and plenums to isolate the test section from the channel blowers and apparatus for measurement of mass flow rates.

Figure 1 additionally shows four heated sections of the channel walls, denoted CC1, CV1, CC2 and CV2. Each of these segments is instrumented with thermocouples to measure channel surface temperatures, etched foil heaters to heat channel surfaces, and insulation to minimize conduction losses [11, 14]. One hundred thermocouples are placed between the heaters and non-flow side of the 0.08 cm Lexan at 10 streamwise locations. These provide sufficient data to calculate spanwise-averaged Nusselt numbers on concave and convex surfaces. At each location, thermocouples are placed in rows of five. The five thermocouples in each row extend across the channel span a distance of 20.32 cm. Rows of thermocouples on the straight portion of the channel are located at x/d of 12, 36, 60, 84 and 108. This first location corresponds to $X = 0.722$ m. Rows of thermocouples on the curved portion of the channel are located at x/d of 132, 156, 180, 204 and 228.

To determine conductive losses from the heated portions of the channel, 40 additional thermocouples are placed in the insulation located behind the etched foil heaters. These thermocouples are placed in pairs along the channel centerline behind each row of thermocouples. This arrangement allows the temperature drop through the insulation to be measured, and the conduction loss to be determined along all segments of the test section. One additional thermocouple is used to measure the mixed mean temperature at the channel inlet.

Data acquisition system

Voltages from the 141 T-type thermocouples are read sequentially using Hewlett-Packard relay multiplexer card assemblies, installed in an HP3497A low-speed Data Acquisition/Control Unit and an

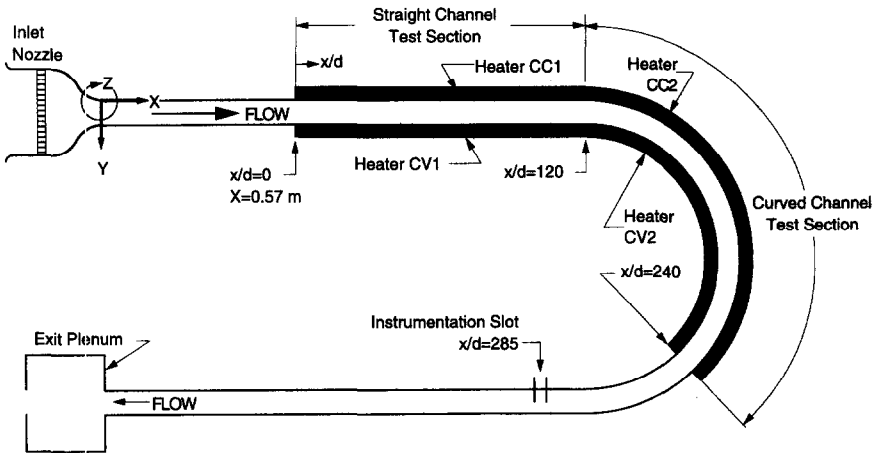

Fig. 1. Channel coordinate system and geometry.

HP3498A Extender. This system provides thermocouple compensation electronically such that voltages for type T thermocouples are given relative to 0°C. A Hewlett-Packard 9836A computer processes signals from all 141 thermocouples to determine local Nusselt numbers using procedures described below.

Nusselt number measurement

Procedures to measure local Nusselt numbers are described by Hedlund [14] and Ligrani *et al.* [11]. Details are also presented here for completeness. After the appropriate air flow rate is established in the channel, all four heaters are adjusted to provide a constant heat flux boundary condition, and the channel is allowed to reach thermal equilibrium. All thermocouple voltages and heater power levels are then measured and converted into surface temperatures and convective heat flux levels $\dot{q}''_{\text{conv}}$.

The latter are given by an equation of the form

$$\dot{q}''_{\text{conv}} = ((IV/5) - \dot{q}_{\text{cond}})/A$$

where I is the electric current through the heater, V is the voltage drop across the heater, A is the surface area of one segment of the heated test section, and $\dot{q}_{\text{cond}}$ is the conductive power lost through the insulation of each heater segment. The power supplied to each heater segment $IV/5$ is one fifth of the total power supplied to each heater. The local heat transfer coefficient is subsequently given by

$$h = \dot{q}''_{\text{conv}}/(t_{\text{w}} - t_{\text{m}}). \tag{1}$$

Local Nusselt number is then given by an equation having the form

$$Nu = hD_{\text{H}}/k. \tag{2}$$

Energy balances are used to determine t_{m}, the local mixed mean temperature at any streamwise channel location in equation (1). The form of the energy balance equation used for this purpose is given by:

$$t_{\text{m}} = t_{\text{m-inlet}} + (\dot{q}''_{\text{conv}} b\,\Delta x)/\dot{m}C_{\text{p}} \tag{3}$$

where $t_{\text{m-inlet}}$ is the mixed mean temperature at the channel inlet, b is the spanwise width of the heated surface, Δx is the streamwise distance from the beginning of heating to the streamwise station of interest, $\dot{m}$ is the air mass flow rate, and C_{p} is air specific heat.

As mentioned earlier, calibrated copper–constantan (T-type) thermocouples are used to determine local wall temperatures at 100 locations along the channel surfaces. Because t_{w} in equation (1) represents the temperature of the surface just adjacent to the air stream, temperatures measured by the thermocouples must be corrected for the 0.08 cm thick Lexan sheet separating each thermocouple from the air stream, as well as the thermocouple-Lexan contact resistance. Corrected wall temperature t_{w} is given by

$$t_{\text{w}} = t_{\text{w-uc}} - C_{\text{R}}\dot{q}''_{\text{conv}} \tag{4}$$

where $C_{\text{R}} = 0.0034°\text{Cm}^2\,\text{W}^{-1}$ determined from experiment, and $t_{\text{w-uc}}$ is the uncorrected temperature measured by each thermocouple.

A number of checks of the experimental apparatus and measurement procedures are conducted. These include checks of Nusselt number spanwise uniformity [11, 14], which is especially good at higher channel Dean numbers (>300), where uniformity within 0.3 Nusselt number units indicates minimal spanwise conduction losses. At Dean numbers less than 45–60, small spanwise variations with Z/d result from natural convection influences [11].

Overall energy balance checks are also conducted at Dean numbers less than 300 [11]. These are accomplished by direct measurements of the local mixed mean temperature just downstream of the heated portion of the channel. This is accomplished using a thermocouple probe to measure local fluid temperature and a miniature five-hole pressure probe [16, 17] to measure local velocity across the channel YZ plane at $x/d = 285$. These direct t_{m} results are then compared to mixed mean temperatures determined from energy balances using equation (3). In all cases, the two measurements of mixed mean temperature agree within a few percent [11]. The agreement verifies the procedures employed to determine spanwise-averaged Nusselt numbers including conduction energy balances and energy balances to calculate mixed-mean temperatures. The experimental uncertainty of Nusselt numbers based on a 95% confidence level is $\pm 4\%$.

Local mean velocity surveys

The miniature five-hole probe, described by Ligrani *et al.* [16], is used to measure total pressure and the three mean velocity components locally at different locations across the cross-section of the transparent curved channel which is employed exclusively for such measurements [3, 12, 13]. The tip diameter of the probe is 1.22 mm to minimize flow blockage and maximize spatial resolution in the confined channel interior. Additional corrections to account for finite spatial resolution and streamline displacement effects are made during data reduction following Ligrani *et al.* [17].

Longitudinal velocity fluctuation surveys

Surveys of streamwise mean velocity and longitudinal velocity fluctuations are obtained using Dantec 55P04 single hot-wire probes. Sensor diameter and length are 5 μm and 1.25 mm, respectively. Each probe is operated at an overheat ratio of 1.8 using a Dantec 55M10 constant-temperature bridge. Individual probes are calibrated in the freestream flow of a wind tunnel using procedures for low velocity measurement described by Ligrani and Bradshaw [18]. These hot-wire probes are mounted in spanwise/radial planes 120° from the start of curvature in the transparent curved channel [3, 12, 13] using the same automated two-dimensional traverse employed for the miniature five-hole pressure probe. Signals are conditioned with

an amplifier gain of 2, a low-pass filter of 1.0 kHz, and no high-pass filter. Data are acquired at 2500 Hz using a Hewlett-Packard 6944A Series 200 Multiprogrammer with a buffered 69759A analog-to-digital conversion card capable of 12-bit binary resolution. This multi-programmer is controlled by a Hewlett-Packard Model 320 Series 9000 Computer, which also stores and processes the data. With this acquisition system, 20000 data samples are obtained at each measurement location which amounts to a sampling interval of 8.0 s.

EXPERIMENTAL RESULTS

Nusselt number characteristics at Dean numbers from 300 to 750 are discussed in this section in reference to Figs. 2–10. Effects of curvature, streamwise development, buoyancy, Dean number, and flow tripping are included in the discussion.

Effects of curvature and streamwise development

Nusselt numbers are presented as dependent upon normalized streamwise distance in Fig. 2 for Dean numbers of 327, 549, 629 and 709. These correspond to Re_d of 2242, 3764, 4312 and 4861, and to Re of 4484, 7528, 8624 and 9722, respectively. Results from the concave and convex surfaces are given at different x/d for each Dean number to illustrate the effects of curvature and streamwise development.

Results from the straight portion of the channel ($0 \leqslant x/d \leqslant 120$), presented in Fig. 2, provide several important checks on the experimental data for all four Dean numbers. First, Nusselt numbers measured on both sides of the channel (labeled concave and convex even though they are on the straight channel segment) are nearly equal at each streamwise location. This

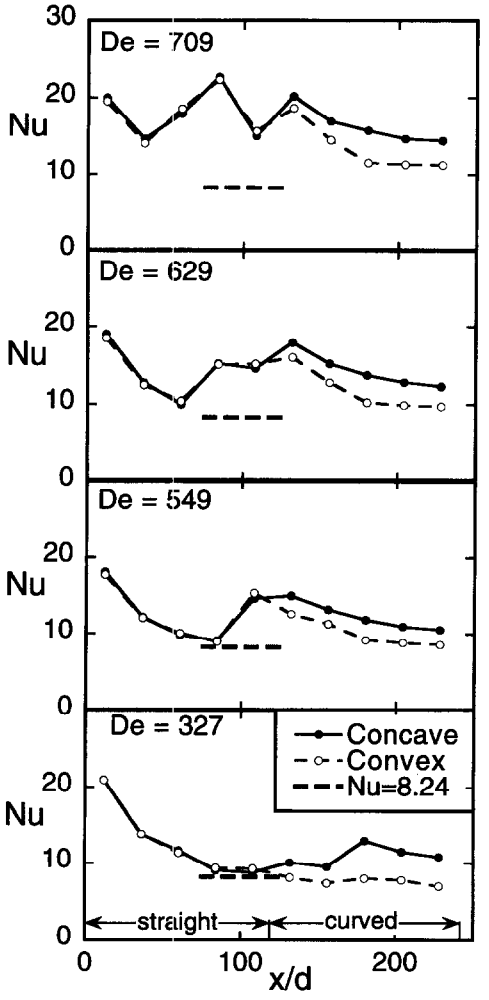

Fig. 2. Forced convection Nusselt numbers as dependent upon x/d for Dean numbers of 327, 549, 629 and 709.

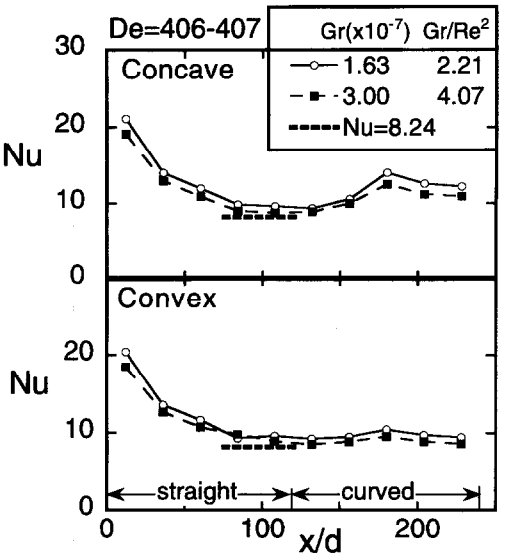

Fig. 3. Effects of buoyancy on mixed convection Nusselt numbers measured at different Gr, Gr/Re^2 and x/d for Dean numbers from 406 to 407.

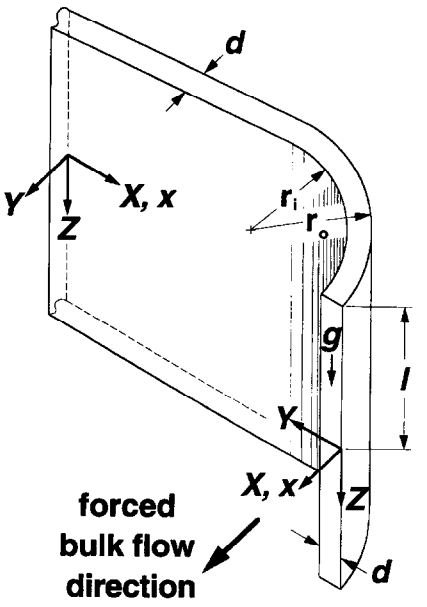

Fig. 4. Channel coordinate system and geometry showing direction of gravitational field.

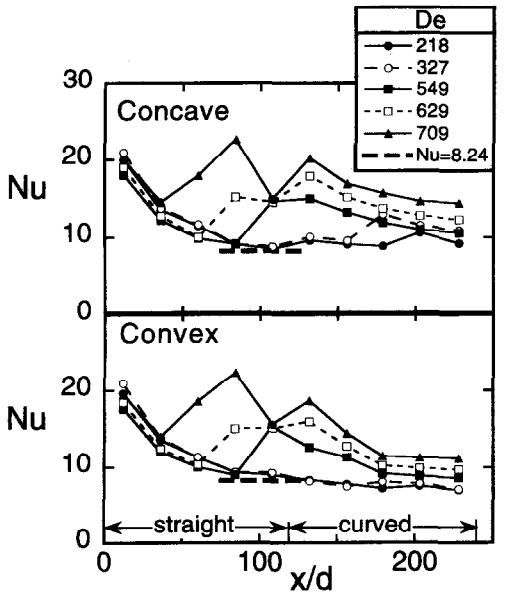

Fig. 5. Forced convection Nusselt numbers as dependent upon x/d for Dean numbers of 218, 327, 549, 629 and 709 for the concave and convex channel surfaces.

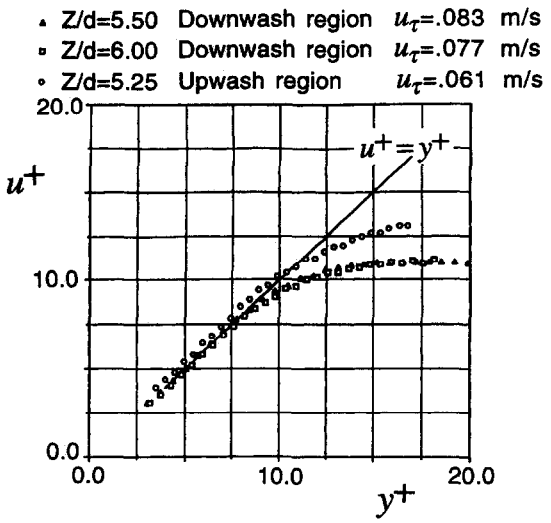

Fig. 6. Normalized streamwise mean velocity profiles at three different spanwise locations at $De = 125$ and $x/d = 219$.

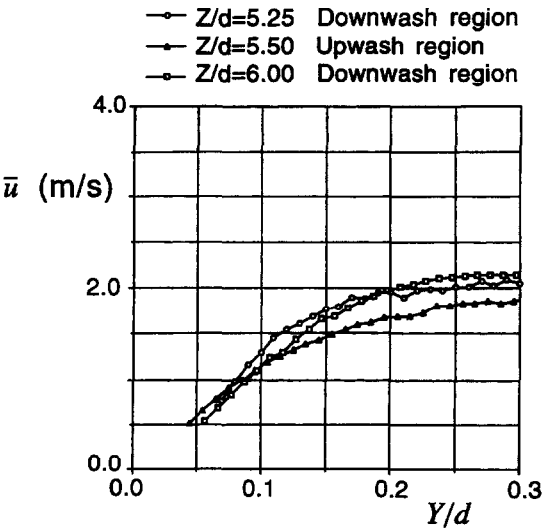

Fig. 7. Normalized streamwise mean velocity profiles at three different spanwise locations at $De = 240$ and $x/d = 219$.

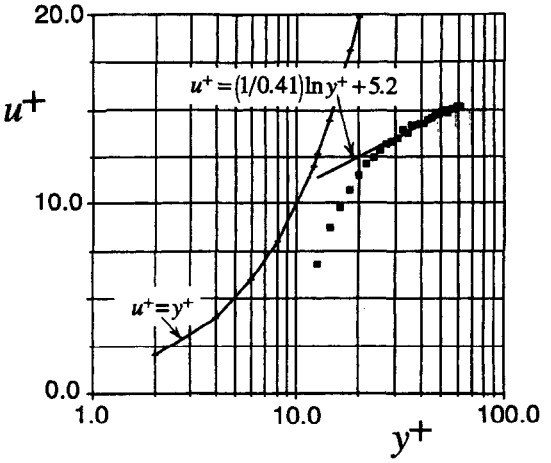

Fig. 8. Normalized streamwise mean velocity profile at $De = 401$ and $x/d = 219$.

evidences two-dimensional velocity and thermal field development, and validates the measurement procedures used. This is additionally important because the flow at the end of the straight channel section, at $x/d = 120$, provides the thermal and velocity inlet conditions for the curved portion of the channel.

A second check is provided by the *trends* of the Nusselt number data with respect to streamwise distance in the straight portion of the channel. For all four Dean numbers, the decrease of Nu with x/d is consistent with thermal boundary layer development upstream of locations where transitional events start to influence the flow. This consistent decrease of Nu occurs from the point on the straight channel where heating begins at $x/d = 0$ to $x/d = 108$ at $De = 327$, $x/d = 84$ at $De = 549$, $x/d = 60$ at $De = 629$, and $x/d = 36$ at $De = 709$. Each of these latter locations thus represents the first streamwise location where transitional effects are first observed in the channel.

The third check is provided by Nusselt number data at $De = 327$ and 549. In both cases, Nu magnitudes near the downstream end of the straight portion of the channel (x/d from 80 to 120 for $De = 327$ and x/d from 80 to 84 for $De = 549$) are near 8.24, the Nusselt number value expected for a spanwise-infinite, straight channel with fully-developed, two-dimensional laminar flow and constant heat flux thermal boundary conditions.

In the curved portion of the channel (x/d from 120 to 240), Nusselt numbers measured on the concave surface are consistently higher than values measured on the convex surface for all four Dean number flow conditions illustrated in Fig. 2. This is due to the

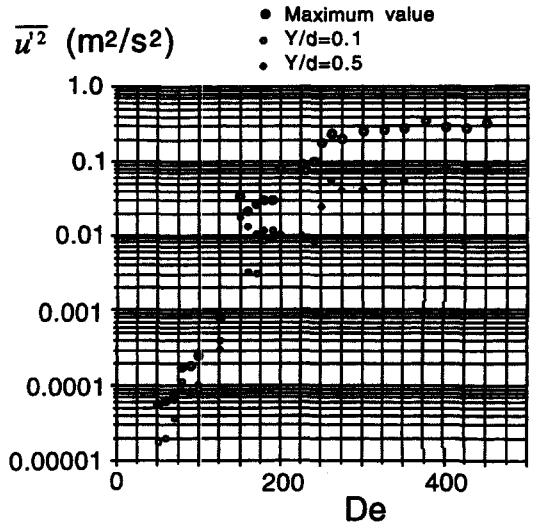

Fig. 9. Variation of the time-averaged magnitude of the square of the longitudinal fluctuating velocity with Dean number at three different locations across the channel cross-section at $x/d = 219$.

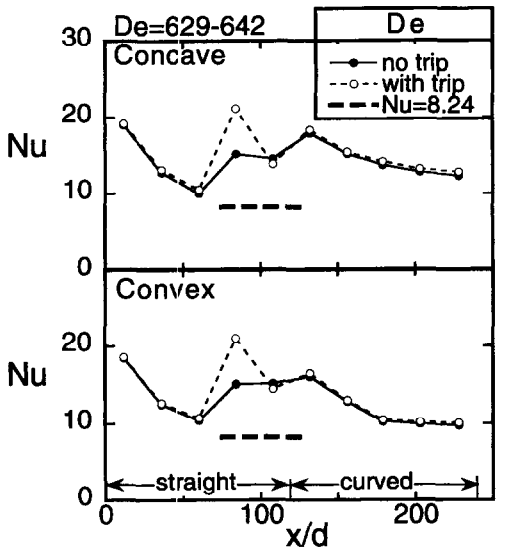

Fig. 10. Effects of tripping on forced convection Nusselt numbers measured at different x/d for Dean numbers from 629 to 642.

unstable stratification of angular momentum in the curved portion of the channel which results in the development of Dean vortex pairs [1–3]. The Dean vortex pairs are generally associated with: (i) more intense secondary flows with greater spatial variations near the concave surface than near the convex surface [3, 12, 13]; and (ii) more unsteadiness [3, 12, 13] near the concave surface than near the convex surface, particularly at Dean numbers greater than 200. Such spatial variations and unsteadiness are generally contained within upwash and downwash regions within vortex pairs (directed away from and towards the concave surface of the channel, respectively, normal to the streamwise direction).

The changes due to curvature are additionally important for all *De* in Fig. 2 because they indicate that the Dean vortex pairs have significant effects on the channel flow despite: (i) the different transitional flow events upstream; and (ii) the resulting different thermal and velocity conditions at the inlet of the curved portion of the channel. Here, transition refers to local or global disturbances or turbulence which result in Nusselt numbers which are higher than values which exist with undisturbed laminar conditions at the same location in the channel. The differences in Nusselt numbers between the concave and convex surfaces (caused by the vortex pairs) are about the same for the different Dean numbers when compared at the same x/d in Fig. 2. One important exception is evident at $De = 327$ as x/d increases from 156 to 180. Here, the local Nusselt number increase which occurs locally as x/d increases is believed to be due to the twisting secondary instability [3, 13]. Twisting is a high intensity vortex rocking motion (when viewed in a streamwise-normal plane), which generally occurs continuously at frequencies between 55 and 90 Hz, with occasional transient occurrences at lower frequencies [3, 13]. Twisting is known to affect *Nu* distributions and local flow behavior at Dean numbers as low as 130–150 depending on the streamwise location in the channel relative to the start of curvature [11, 13].

The section on Nusselt number measurement indicates that local Nusselt number values are spanwise uniform within 0.3 Nusselt number units at each streamwise location investigated. At locations downstream of the initial appearance of transition, this is because of significant amounts of unsteadiness of the Dean vortex pairs and other flow structures, which 'smear' flow structure near the wall.

Effects of buoyancy

The effects of buoyancy on measured Nusselt numbers are illustrated by results presented in Fig. 3. A schematic of the channel illustrating the direction of the gravitational field relative to the coordinate system is shown in Fig. 4. In Fig. 3, data for $De = 406$–407 are given for Grashof numbers ranging from 1.63×10^7 to 3.00×10^7, which are equivalent to Gr/Re_d^2 ranging from 2.21 to 4.07. These Gr/Re_d^2 values are significantly less than the $Gr/Re_d^2 = 50$ boundary between mixed convection with strong buoyancy and mixed convection with weak buoyancy given in Ligrani and Choi [19]. Consequently, these variations of Gr/Re_d^2 represent extremely weak buoyancy influences on *overall* channel behavior, which indicates that buoyancy has little influence on *global* thermal flow field behavior.

This is consistent with the Nusselt numbers in Fig. 3 which show little variation with Gr or Gr/Re_d^2 over the range of x/d measured. A slight *Nu* decrease is evident at each x/d for both channel surfaces as Gr and Gr/Re_d^2 increase, which is qualitatively consistent

with results obtained at lower Dean numbers [19]. With those experimental conditions, the same arrangement of buoyancy behaves qualitatively similarly to buoyancy which is aligned with and in opposition to the forced flow. The small Nu changes with Gr/Re_d^2 occur in Fig. 3 because of the influences of buoyancy *locally* very near walls, at small x/d where streamwise velocities from the forced flow are low with respect to buoyancy induced spanwise velocities, and thermal boundary layers are thin and just beginning to develop. Slight variations in initial thermal boundary layer development occur with different Gr/Re_d^2, producing slightly different initial conditions for the thermal boundary layers which subsequently develop along the channel. The fact that these buoyancy influences on Nusselt number behavior are small is further evidenced by the data in Fig. 3. There, all four Nusselt number data sets (CC1, CV1, CC2, CV2) approach the forced flow Nu value of 8.24 as thermal layers become fully developed near the downstream end of the straight portion of the channel at x/d from 80 to 120.

The Nusselt number data in Fig. 3 for $Gr/Re_d^2 = 2.21$–4.07 thus *largely* represent pure forced convection behavior. Grashof numbers for the data in Fig. 2 range from 4.5×10^7 to 5.0×10^7 which gives Gr/Re_d^2 from 1.9 to 9.9. These low Gr/Re_d^2 values relative to $Gr/Re_d^2 = 50$ [19] also indicate minimal buoyancy influences on *global* thermal behavior which means that the data in Fig. 2 also largely represent pure forced convection behavior. (Note that no data are available for $De = 406$–407 and $Gr = 4.5$–5.0×10^7). If buoyancy influences thermal boundary layer behavior in these flows, it does so locally only at small x/d where thermal boundary layers are thin and just beginning to develop [11, 19], as mentioned earlier. Changes farther downstream, if they occur, then result because the initial profile for thermal boundary layer development is altered. This is borne out by the measurements at $De = 406$–407, and is some cases, by local Nu data at Dean numbers as high as 709.

Effects of Dean number

The results from Fig. 2 are again plotted in Fig. 5 along with one additional Nusselt number data set for $De = 218$. In the top portion of Fig. 5, data measured on the concave surface for all Dean numbers are plotted together, and in the bottom portion of Fig. 5, data measured on the convex surface for all Dean numbers are plotted together.

The Nusselt number data in Fig. 5 for $De = 218$ and 327 represent pure laminar behavior in the straight portion of the channel ($0 < x/d < 120$). Here, Nu values first decrease with x/d and then become approximately constant with $x/d = 80$–120, where Nusselt number values are close to 8.24. Dean vortex pairs form soon after the flow enters the channel at x/d just greater than 120 [3]. As this occurs, Nusselt numbers from the concave surface become greater than values at the same streamwise location on the convex surface [11]. After this occurs, the vortex pairs undulate [13], split [12], and merge [12] at x/d from about 130 to values as high as 180, with almost no additional Nusselt number variations with x/d. With additional downstream development at $De = 218$ and 327, the twisting secondary instability develops [13], and produces important Nusselt number increases on the concave surface relative to the convex surface [11]. These increases are evident in Fig. 5 for concave surface Nusselt numbers only as x/d increases from 180 to 204 at $De = 218$, and as x/d increases from 156 to 180 at $De = 327$.

Examples of velocity profiles measured with laminar flow and Dean vortex pairs in the channel are presented in Fig. 6. These data are measured at $De = 125$ and $x/d = 219$ near the downstream end of the curved portion of the channel. The linear behavior, which characterizes purely laminar behavior and no turbulent shear stresses near the channel surfaces, is evident for $y^+ < 10$. Streamwise mean velocities are lower in the upwash region than in the downwash region. However, in the normalized coordinates in Fig. 6, normalized upwash region velocities are higher due to locally lower friction velocity. Dimensional streamwise mean velocity profiles measured with twisting Dean vortex pairs in the channel are presented in Fig. 7 for $De = 240$ and $x/d = 219$. Higher velocities in the downwash region and relatively lower velocities in the upwash region are apparent, which illustrates that time-averaged variations in the vortex pairs exist in spite of the unsteadiness from twisting [13]. The spanwise locations of upwash regions and portions of downwash regions are at different Z/d in Figs. 6 and 7 because time-averaged locations of Dean vortex pairs shift as the Dean number changes [3, 12, 13].

From the results in Fig. 5, it is apparent that the twisting secondary instability is very important in initiating the transition process in curved channels. When twisting is present, the most intense spatial and temporal variations of secondary flows are present near the concave surface, particularly in upwash regions located between the vortices in each pair [13]. As a result, concave Nu are significantly higher than Nu from the convex surface at the same x/d [11]. Transitional events such as twisting occur at the downstream end of the channel after Dean vortex pairs are already present and well developed. Other transitional events then occur at locations which are progressively upstream as the Dean number increases.

As the Dean number increases to reach 549, Fig. 5 shows that Nusselt numbers on both the concave and convex channel surfaces are significantly higher than values measured at $De = 218$. The straight portion of the channel then remains fully laminar up to $x/d = 84$. As x/d then increases, transitional events develop at x/d from 84 to 108 and are then present throughout the curved portion of the channel causing Nusselt numbers on concave and convex surfaces to increase (relative to values at lower De). A normalized velocity

profile presented in Fig. 8 for similar conditions ($De = 401$) shows late transitional 'turbulent-like' behavior at the downstream end of the curved portion of the channel ($x/d = 219$), which probably indicates that most transitional events occurred upstream.

Figure 5 further shows that the Nusselt number trend continues as the Dean number increases even further to $De = 629$ and 709, since Nusselt numbers continue to increase with De at each x/d. In addition, the location where transitional events cause initial Nusselt number increases, relative to pure laminar values, moves farther upstream. As a result, pure laminar Nusselt number behavior is present in the straight portion of the channel only up to $x/d = 60$ at $De = 629$ and only up to $x/d = 36$ at $De = 709$.

The types of transitional events responsible for the Nusselt number increases relative to pure laminar values in Figs. 2 and 5 (especially for De of 549, 629 and 709) are probably similar to ones which nominally occur in straight pipes and channels with transitional flow. The most important events are 'slugs' and 'puffs' of turbulence [4, 5]. According to Stettler and Hussain [4], 'slugs' originate from instability waves of entry region boundary layers, whereas 'puffs' are 'debris of relaminarization of fully turbulent flow induced at the entry by large disturbances or roughness (which can be an orifice, grid, disc, etc.)'. The instabilities which produce 'slugs' include modified Tollmein–Schlichting waves which are often followed or accompanied by packets of small longitudinal vortices in near-wall boundary layer regions. 'Puffs' and 'slugs' thus both often appear in pipes and channels as longitudinally separated regions of turbulence. Something similar to these events, most probably 'slugs', is speculated to be occurring quite frequently in the straight portion of our channel at $De > 400$ at locations evidenced by local Nusselt number increases with x/d relative to values for two-dimensional laminar channel flow. As mentioned earlier, these initial transitional flow events are located progressively upstream through the straight portion of the channel as De increases from 400 to 709. These produce disturbances which then advect downstream by different distances as the Dean number changes to produce different initial conditions at the entrance of the curved portion of the channel at $x/d = 120$.

Variations of time-averaged magnitudes of the square of the fluctuating velocity, $\overline{u'^2}$, provide additional insight into curved channel transition. The results presented in Fig. 9 are obtained in a cross-sectional plane located at $x/d = 219$, which covers Z/d from 4 to 8 and Y/d from 0.1 to 0.8. Maximum $\overline{u'^2}$ values are shown along with values measured in the upwash region of a vortex pair at $Y/d = 0.1$ and $Y/d = 0.5$. The $\overline{u'^2}$ increases which occur as Dean number increases from 0 to 150 occur mostly from: (i) unsteadiness as the vortices initially form near the concave surface as tiny Görtler vortices and are particularly sensitive to small amplitude perturbations and spanwise wave number selection [3, 12]; (ii) undulating motions [13]; (iii) splitting, merging, and spanwise wave number selection of fully formed vortex pairs [12]; and (iv) unsteadiness from random perturbations occurring at the channel inlet [3, 12, 13]. The $\overline{u'^2}$ variations shown in Fig. 9 at De from 130 to 200 are due to twisting [13]. Here, significant $\overline{u'^2}$ are present only within upwash regions between the vortices in each pair where twisting motions are initially most intense. The maximum $\overline{u'^2}$ which occur within these upwash regions are located between $Y/d = 0.1$ and $Y/d = 0.5$.

At Dean numbers between 200 and 300, twisting probably continues to be present, $\overline{u'^2}$ continues to increase with De, and the maximum $\overline{u'^2}$ in the cross-sectional plane measured occurs at $Y/d = 0.1$. Time-averaged surveys of $\overline{u'^2}$ at these conditions continue to show regions with locally increased $\overline{u'^2}$ magnitudes located within the near vortex pair upwash regions. Afterwards, at higher De, the late-transitional 'turbulent-like' behavior, characterized by the mean velocity profile in Fig. 8 is present. Time-averaged turbulence structure is then more spanwise uniform [13], and $\overline{u'^2}$ increases only very gradually with Dean number at each cross-sectional plane location.

In spite of such small $\overline{u'^2}$ changes with De, Nusselt numbers in Fig. 5 continue to increase with De at $x/d = 219$ for $De > 250$. In addition, concave surface Nusselt numbers in Fig. 2 are higher than convex surface values at De as high as 709, which means that Dean vortex pairs continue to be present and continue to affect thermal flow behavior in a significant way. Both of these Nusselt number characteristics further suggest that the thermal boundary layers responsible for the Nusselt number variations are dependent upon upstream initial conditions for development, transitional disturbances and levels of turbulence intensity very near the measurement location.

Effects of tripping the flow

All experimental data presented thus far are obtained with no trips placed near the channel inlet. Here, however, Nusselt number results in Fig. 10 are described for $De = 629$–642, which are obtained with 2 mm high trips placed just upstream of the straight portion of the channel on both channel surfaces. Each trip is spread across the span of the channel inlet, and located $72d$ upstream of $x/d = 0$, the streamwise location where channel heating begins. The data obtained with trips are compared to results obtained with no trips, at similar conditions, to provide indications of events altered by the presence of near wall disturbances. Local Nusselt number variations from transitional events, in particular, can be altered by such small-scale disturbances and thus sometimes changed when the channel flow is tripped. The disturbances from the trips probably result in turbulent 'puffs' [4, 5], rather than turbulent 'slugs' [4, 5] because of the nature of the small separated and recirculating flow regions located just downstream of the trips.

Nusselt number distributions, obtained with and without trips, are presented in Fig. 10 for $De = 629$–642. Here, the most important local Nusselt numbers increase from tripping is evident at x/d between 60 and 108 and especially noticeable at $x/d = 84$. The increase occurs as Nusselt numbers first deviate from pure laminar values near $x/d = 60$, which may suggest an initial local increase in the frequency and/or intensity of localized 'puffs' of turbulence. Tripped Nusselt numbers become closer to untripped values as x/d becomes greater than 108. As the tripped flow enters the curved section of the channel at $x/d = 120$, local Nu data are then just slightly greater than untripped Nusselt number data. Thus, the effects of the local disturbances produced by the trips on local Nusselt numbers subside with streamwise development, and are then overwhelmed by the secondary flows induced by curvature at $x/d > 120$.

Tripped Nusselt number distributions show qualitative trends (relative to untripped flows) similar to the ones shown in Fig. 10 at a Dean number of 709 [14]. Effects of tripping are also evident in Nusselt number data at some experimental conditions when the Dean number is lower than 629–642 [14].

SUMMARY AND CONCLUSIONS

At Dean numbers from 300 to 750, Nusselt numbers measured on the concave surface are significantly higher than values measured on the convex surface at x/d from 120 to 240 in the curved portion of the channel. Thus, Dean vortex pairs are not only believed to be present in the channel at these Dean numbers, but they also strongly influence thermal flow field behavior. Overall Nusselt number variations with x/d and De also suggest that the thermal boundary layers responsible for the Nusselt number variations are dependent upon upstream initial conditions in addition to transitional disturbances and levels of turbulence intensity very near the measurement location. These initial conditions are the result of different transitional flow events in the upstream straight portion of the channel, and the thermal and velocity conditions at $x/d = 120$ at the inlet of the curved portion of the channel.

Important Nusselt number increases from these transitional events are evident in the straight portion of the channel at x/d from 12 to 54 at the Dean number increases from about 500 to 750. These events affect the straight channel thermal field such that Nusselt number variations are the same on both channel surfaces at a particular x/d. The Nusselt number increases are believed to be due to local transitional 'slugs' or 'puffs' of turbulence [4, 5]. These cause initial Nusselt number augmentations relative to pure laminar values to be located progressively upstream as the Dean number increases.

Trips provide indications of events altered by the presence of near wall disturbances initiated at the inlet of the straight portion of the channel. At $De = 629$–642, the influences of trips on the thermal field, as evidenced by local Nusselt number variations in the channel, are localized to x/d between 60 and 108, and then overwhelmed by the secondary flows induced by curvature at $x/d > 120$.

Although the buoyant effects examined here are extremely weak, the slight increase in local Nusselt number with increasing Grashof number is believed to be due to buoyancy induced spanwise velocity in a region of the channel in which the thermal boundary layer is just beginning to develop, and is still very thin. This produces a slight increase in Nusselt numbers throughout the channel which are believed to result from a change in thermal profile development throughout the channel.

Surveys of streamwise mean velocity and time-averaged magnitudes of the square of the fluctuating velocity, $\overline{u'^2}$, measured in a cross-sectional plane located at $x/d = 219$, also provide additional insight into curved channel transition.

Acknowledgements—This work was sponsored by the Propulsion Directorate, U.S. Army Aviation Research and Technology Activity-AVSCOM, through NASA-Defense Purchase Request C-30030-P. The program monitor was Mr Kestutis Civinskas.

REFERENCES

1. Dean, W. R., Fluid motion in a curved channel. *Proceedings of the Royal Society of London, Series A*, 1928, **121**, 402–420.
2. Brewster, D. B., Grosberg, P. and Nissan, A. H., The stability of viscous flow between horizontal concentric cylinders. *Proceedings of the Royal Society of London, Series A*, 1959, **251**, 76–91.
3. Ligrani, P. M. and Niver, R. D., Flow visualization of Dean vortices in a curved channel with 40 to 1 aspect ratio. *Physics of Fluids*, 1988, **31**, 3605–3617.
4. Stettler, J. C. and Hussain, A. K. M. F., On transition of the pulsatile pipe flow. *Journal of Fluid Mechanics*, 1986, **170**, 169–197.
5. Ligrani, P. M., Subramanian, C. S., Coumes, T. M., Greco, F. J., Koth, H. and Longest, J. M., Study of the imposition of bulk flow pulsations on plane channel flow at moderate Stokes numbers. *Experimental Thermal and Fluid Science*, 1992, **5**, 145–161.
6. Cheng, K. C. and Akiyama, M., Laminar forced convection heat transfer in curved rectangular channels. *International Journal of Heat and Mass Transfer*, 1970, **13**, 471–490.
7. Mori, Y., Uchida, Y. and Ukon, T., Forced convective heat transfer in a curved channel with a square cross-section. *International Journal of Heat and Mass Transfer*, 1971, **14**, 1787–1805.
8. Yee, G., Chilukuri, R. and Humphrey, J. A. C., Developing flow and heat transfer in strongly curved ducts of rectangular cross-section. *ASME Transactions—Journal of Heat Transfer*, 1980, **102**(2), 285–291.
9. Chilukuri, R. and Humphrey, J. A. C., Numerical computation of buoyancy induced recirculation in curved square duct laminar flow. *International Journal of Heat and Mass Transfer*, 1981, **24**, 305–314.
10. Komiyama, Y., Laminar forced convection heat transfer in curved channels of rectangular cross-section. *Transactions of The Japan Society of Mechanical Engineers B*, 1984, **50**(450), 424–434.

11. Ligrani, P. M., Choi, S., Schallert, A. R. and Skogerboe, P. E., Effects of Dean vortex pairs on surface heat transfer in curved channel flow. *International Journal of Heat and Mass Transfer*, 1996, **39**(1), 27–37.
12. Ligrani, P. M., Longest, J. E., Kendall, M. R. and Fields, W. A., Splitting, merging and spanwise wavenumber selection of Dean vortex pairs. *Experiments in Fluids*, 1994, **18**(1), 41–58.
13. Ligrani, P. M., Finlay, W. H., Fields, W. A., Fuqua, S. J. and Subramanian, C. S., Features of wavy vortices in a curved channel from experimental and numerical studies. *Physics of Fluids A*, 1992, **4**(4), 695–709.
14. Hedlund, C. R., Effects of transition to turbulence and Dean vortex pairs on surface heat transfer in curved and straight channels at moderate and high Dean numbers. M.S. thesis, University of Utah, Salt Lake City, Utah, 1996.
15. Incropera, F. P. and De Wit, D. P., *Introduction to Heat Transfer*, 2nd edn. Wiley, New York, 1990.
16. Ligrani, P. M., Singer, B. A. and Baun, L. R., Miniature five-hole pressure probe for measurement of mean velocity components in low speed flows. *Journal of Physics E—Scientific Instruments*, 1989, **22**(10), 868–876.
17. Ligrani, P. M., Singer, B. A. and Baun, L. R., Spatial resolution and downwash velocity corrections for multiple-hole pressure probes in complex flows. *Experiments in Fluids*, 1989, **7**(6), 424–426.
18. Ligrani, P. M. and Bradshaw, P., Subminiature hot-wire sensors: development and use. *Journal of Physics E—Scientific Instruments*, 1987, **20**, 323–332.
19. Ligrani, P. M. and Choi, S., Mixed convection in straight and curved channels with buoyancy orthogonal to the forced flow. *International Journal of Heat and Mass Transfer*, 1996, **39**(12), 2473–2484.